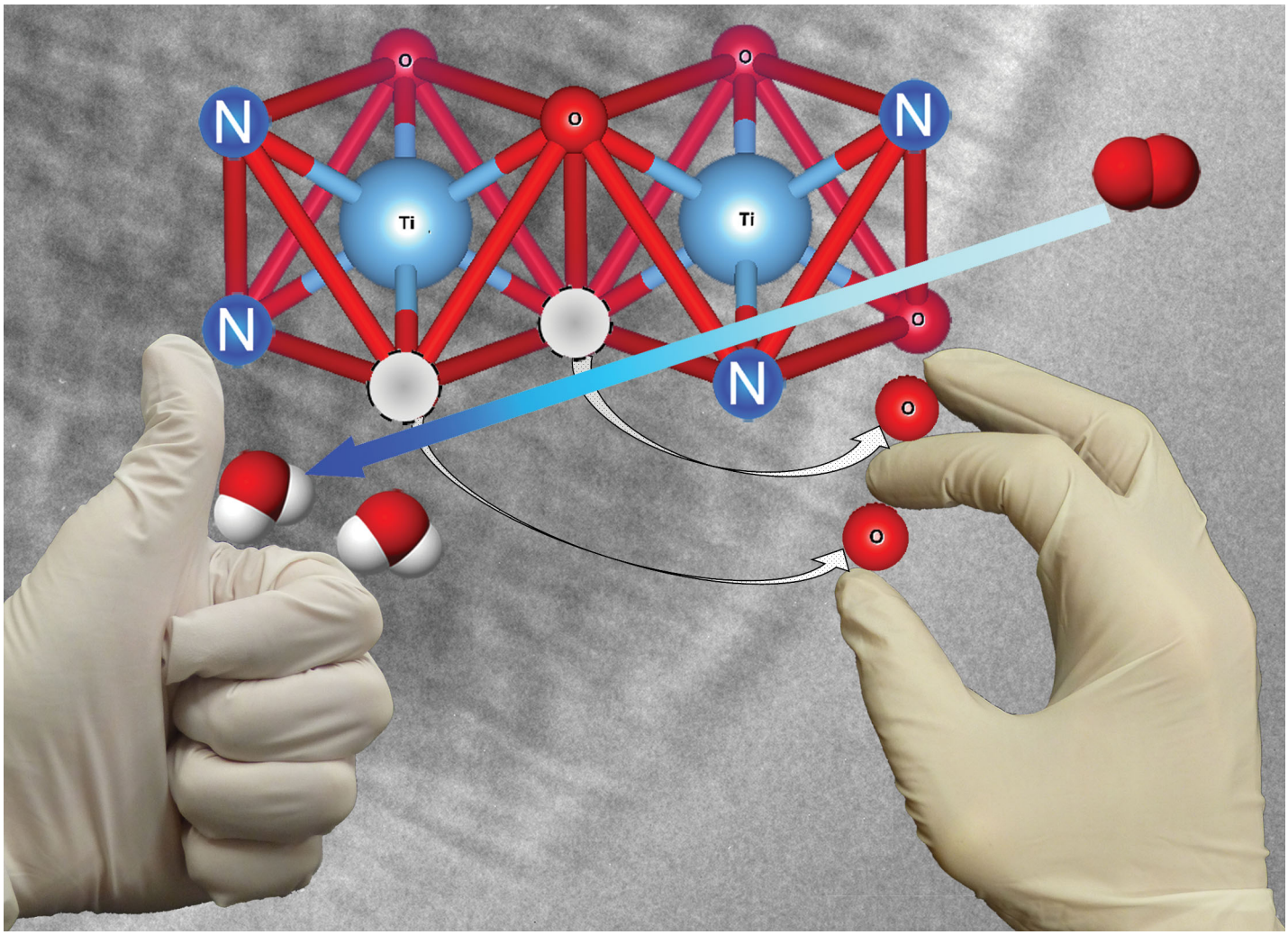

Showcasing work on titanium oxynitride fuel cell catalysts by Prof. Chisaka at Hirosaki University, Japan.

Creation of oxygen reduction reaction active sites on titanium oxynitride without increasing the nitrogen doping level

Active sites for the oxygen reduction reaction on carbon-support-free titanium oxynitride catalysts were created without increasing the surface nitrogen doping level, while changing the number of oxygen vacancies on the rutile TiO_2 covered surface of the TiN-core. The developed low temperature annealing approach revealed that the oxygen vacancies definitely produced the active sites for oxygen reduction reaction in acidic media.

As featured in:

See Mitsuharu Chisaka, *Phys. Chem. Chem. Phys.*, 2018, **20**, 15613.

ROYAL SOCIETY OF CHEMISTRY

rsc.li/pccp

Registered charity number: 207890

PCCP

COMMUNICATION

View Article Online
View Journal | View Issue

Cite this: *Phys. Chem. Chem. Phys.*, 2018, **20**, 15613

Received 4th March 2018,
Accepted 12th April 2018

DOI: 10.1039/c8cp01420e

rsc.li/pccp

Creation of oxygen reduction reaction active sites on titanium oxynitride without increasing the nitrogen doping level†

Mitsuharu Chisaka

The oxygen reduction reaction (ORR) active sites on titanium oxynitride (TiO_xN_y) have been investigated using catalysts with various nitrogen doping levels, leaving some margins to determine their origin. Herein, low-temperature annealing enhanced the ORR activity of carbon-support-free TiO_xN_y with a constant nitrogen doping level, indicating that oxygen vacancies produced the sites.

Due to the worldwide trend to mandate the reduction of vehicle emissions, both lithium-ion batteries (LIBs) and polymer electrolyte fuel cells (PEFCs) have attracted increasing attention as power sources to replace internal combustion engines. The advantages of PEFCs are a facile fuelling time of several minutes and a high power density estimated to be $\sim$1.2–1.8 W cm^{-2} of electrodes in commercial vehicles.[1] Therefore, in particular, PEFCs are the best alternatives for vehicles carrying high loads, *e.g.* buses and trucks, as well as for those travelling long distances over 300 miles[2] because in these vehicles, both the mass and the volume of the PEFC system are much lower than those of their LIB counterparts.[2,3] PEFCs utilise proton exchange membranes and ionomers as electrolytes and binder/proton conductors in catalyst layers, respectively. Hence, catalysts are under highly acidic conditions due to abundant protons. Besides, cathode catalysts are exposed to high potentials, 0.6–1.0 V *versus* the reversible hydrogen electrode (RHE) in vehicles.[4] These oxidative operating conditions and the slow kinetics of the oxygen reduction reaction (ORR) require a huge amount of scarce and expensive platinum-based catalysts at PEFC cathodes.

The above-mentioned oxidative environments have been a barrier to the development of stable and active platinum group metal (PGM)-free cathode catalysts. In an alkaline environment, some non-PGM catalysts have exhibited a higher ORR activity in comparison with commercial carbon-supported platinum catalysts[5–7] even at identical catalyst loadings,[6] whereas such a high ORR activity has not been reported in acidic PEFC cathodes. Significant efforts have been made to determine the ORR active sites on the most widely developed non-PGM catalyst type for the PEFC cathode, *i.e.* Fe(Co)/N/C, which comprises iron/cobalt, nitrogen and carbon atoms.[8] Some controversial discussions on several proposed active sites still continue, whereas most recent studies have focused on increasing both the number and density of the sole active site, *i.e.* iron/cobalt atoms coordinated with nitrogen atoms at the edge of graphitic carbons to enhance the ORR activity.[7,9] There have been insufficient studies investigating the ORR active sites for another non-PGM catalyst type, group IV or V metal oxide compounds, for proposing only anion vacancies in both acidic and alkaline media.[10–15] The vacant site can be created using several methods, *e.g.* simple reduction using annealing, carbothermal reduction, substitution of group IV or V metals by cations with a lower valence and substitution of oxygen by an anion with a lower valence. Recent progress on activity enhancement was achieved by the last method, *i.e.* substitutional nitrogen doping into titanium oxide[13–15] or zirconium oxide[16] to create oxygen vacancies. In particular, we recently investigated carbon-support-free nitrogen-doped titanium oxide[14,15] as it is promising in terms of both the ORR activity and stability. The bulk of the catalyst was TiN, and the surface was oxidised to form amorphous or rutile TiO_2 with nitrogen atoms, hereinafter referred to as titanium oxynitride (TiO_xN_y). The surface valence of titanium was mostly 4, and oxygen vacancies were produced to compensate for the charge imbalance caused by the doped nitrogen atoms. The ORR activity of both carbon-supported and carbon-support-free TiO_xN_y catalysts increased with the content of surface nitrogen, which substituted the oxygen atoms in the TiO_2 lattice. Moreover, it was hypothesised that the active site was the result of the oxygen vacancy created by substitutional nitrogen doping.[13–15] Oxygen vacancy is one of the possible sites for the adsorption of oxygen molecules, the first step for the ORR. Indeed, Lyubinetsky *et al.* reported the dissociative adsorption of oxygen molecules on bridging oxygen vacancies on the (110) plane of rutile TiO_2 at room temperature using *in situ* scanning tunnelling microscopy (STM) in 2008.[17]

Department of Sustainable Energy, Hirosaki University, 3 Bunkyo-cho, Hirosaki, Aomori 036-8561, Japan. E-mail: chisaka@hirosaki-u.ac.jp

† Electronic supplementary information (ESI) available: Experimental details, FE-SEM images and ORR kinetic data. See DOI: 10.1039/c8cp01420e

One of the oxygen atoms of O_2 healed one oxygen vacancy, while the other was deposited on a five-fold titanium atom next to the vacancy. Two years later, they also presented another model on the same rutile (110) plane using STM and density functional calculations; oxygen molecules adsorbed on titanium rows, while the charge from the oxygen vacancy promoted the dissociation of oxygen molecules.[18] The dissociative adsorption of oxygen molecules on the (110) plane of rutile TiO_2 with an oxygen vacancy was also reported using STM by Wendt *et al.*, although the proposed source of charges to promote O_2 dissociation was different.[19] These are thought-provoking studies for discussing the ORR active sites on our TiO_xN_y. However, the material reported in the aforementioned studies was nitrogen-free TiO_2 and STM experiments were conducted in an ultra-high-vacuum system free from protons,[17–19] which was different from the acidic media where the ORR activity of TiO_xN_y was evaluated.[13–15] It is difficult to conduct similar STM experiments under realistic PEFC conditions in the presence of acidic electrolytes. Furthermore, in comparison to titanium and oxygen, nitrogen is a foreign atom with a different electronegativity. Nitrogen doping into the TiO_2 lattice induces not only oxygen vacancy formation but also changes in the electronic band structure and charge density. These important factors depend on the chemical states, *i.e.* the site of the doped nitrogen, which is either substitutional or interstitial.[20] Thus, the ORR active sites on TiO_xN_y are still under debate. This is due to the shorter developing period of this catalyst compared with Fe/N/C,[21] which should therefore be investigated to enhance the activity by creating a high active site density on the surface. Investigations into the active sites of TiO_xN_y should be conducted without changing the amount and chemical states of the doped nitrogen atoms in order to distinguish the contribution of the oxygen vacancy from that of the nitrogen atoms.

Herein, for the first time, active sites were created by reducing the ORR active TiO_xN_y without changing the surface nitrogen content and chemical states to identify the origin of sites. The solution-phase combustion route was used to synthesise TiO_xN_y catalysts without supports (S1, ESI†). The route was selected because it did not require carbon supports to evaluate the activity of TiO_xN_y, and carbon residues from the precursor have already been confirmed to contribute to neither activity nor conductivity.[15] Pyrolysis of precursor mixtures at 1123 K under N_2 gas was followed by annealing under a flowing gas mixture of 10% H_2 in Ar at various temperatures that were lower than the initial temperature in the range of 623–1023 K. Annealing did not clearly change the morphology, as observed in field-emission scanning electron microscopy (FE-SEM) images (S2, ESI†), suggesting that aggregation during this process was marginal.

Furthermore, the bulk crystal structure characterised by X-ray diffraction (XRD) did not undergo significant changes when the temperature was maintained below 823 K (Fig. 1). The single-TiN phase was not altered when the temperature was increased to 823 K, whereas weak peaks assigned to the rutile TiO_2 phase appeared at a higher temperature, exhibiting TiO_xN_y oxidation. When carbon-supported hafnium oxynitride

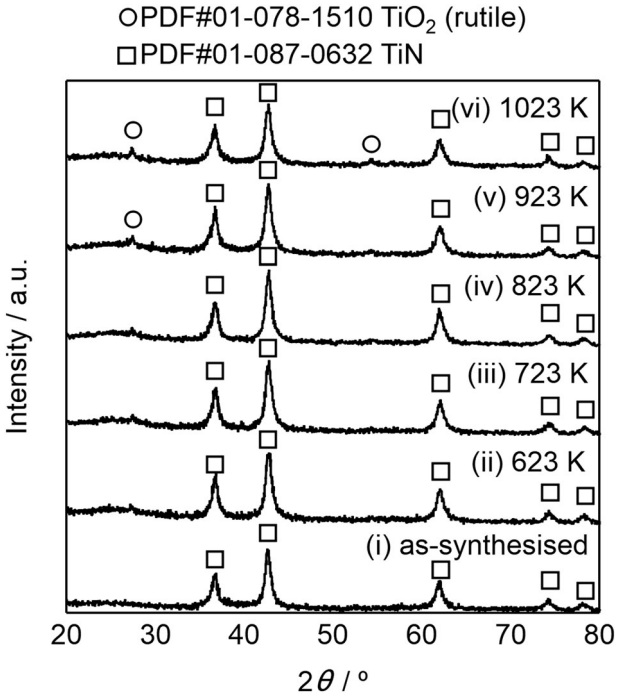

Fig. 1 X-ray diffraction (XRD) patterns of (i) as-synthesised titanium oxynitride (TiO_xN_y) catalysts and of those after annealing at (ii) 623 K, (iii) 723 K, (iv) 823 K, (v) 923 K and (vi) 1023 K under 10% H_2 (v/v) in Ar.

catalysts were annealed under a similar reductive gas, 5% H_2 in Ar, at a considerably higher temperature of 1223 K, oxidation was more severe. All nitrogen atoms were removed to change the crystal structure from the cubic Hf_2ON_2 phase to the monoclinic HfO_2 phase.[22] Herein, at temperatures $\geq$923 K, some nitrogen atoms in TiO_xN_y were removed in the absence of a reactive nitrogen source. A small amount of contaminated oxygen molecules in the mixed gas was assumed to be the source of oxidation during the annealing. Although a small amount of rutile TiO_2 phase appeared at high temperature, the bulk crystal structure of the present TiO_xN_y catalyst series was mostly the well-known conductive nitride, TiN, which was recently revealed to be necessary to evaluate the activity without carbon additives.[15]

The effect of annealing on the surface chemical states was different from that on the bulk crystal structure. Fig. 2 shows the X-ray photoelectron (XP) spectra of the TiO_xN_y catalysts. Both hydrocarbon contaminants from the spectrometer and TiO_xN_y should have contributed to the O 1s spectra, and their contributions could not be distinguished from each other. Therefore, Ti 2p and N 1s spectra were used for the chemical state analyses of TiO_xN_y. The annealing changed the Ti 2p spectrum even at the lowest temperature of 623 K, as shown in Fig. 2(i) and (ii). The Ti 2p level splits into the Ti $2p_{3/2}$ and $2p_{1/2}$ sublevels *via* spin–orbit coupling, displaying doublets in the spectra. Both TiO_xN_y catalysts, before and after annealing, exhibited asymmetric doublets, thereby indicating the presence of several chemical states. The Ti 2p peaks were deconvoluted into three components[13–15] and the fitting results are shown in Fig. 3(a). The binding energy of the main peaks in the Ti $2p_{3/2}$

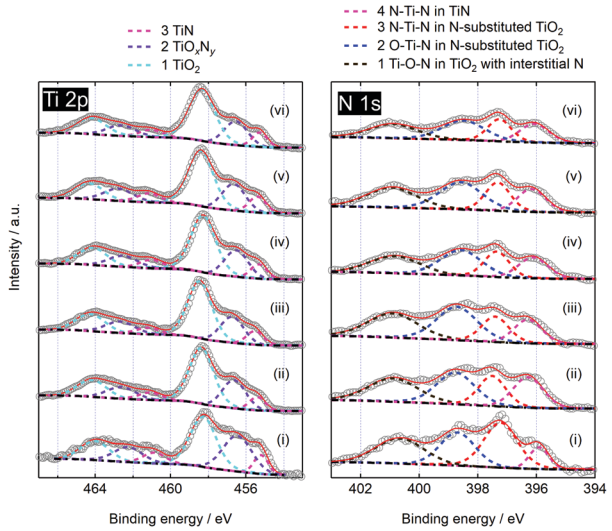

Fig. 2 X-ray photoelectron (XP) Ti 2p and N 1s spectra of (i) as-synthesised TiO_xN_y catalysts and of those after annealing at (ii) 623 K, (iii) 723 K, (iv) 823 K, (v) 923 K and (vi) 1023 K under 10% H_2 (v/v) in Ar. All the spectra (○) are shown with overall fitting (solid line) and deconvolution into several peaks (dashed line) after subtracting a Shirley-type background (dash-dotted line).

region was the same for these two catalysts, *i.e.* ~458.4 eV, and both these main peaks were assigned to Ti^{4+} in TiO_2,[14,15,23] indicating that the surface of TiN was oxidised. The oxidation degree of the two catalysts was different. The area fraction of the satellite peaks at ~457 eV; s_{T2}, which was assigned to TiO_xN_y,[14,15,23] decreased after the 623 K-annealing as shown in Fig. 3(a). Consequently, the 623 K-annealing changed the chemical states of the doped nitrogen atoms. The N 1s peaks were deconvoluted into four components[14,15] and the fitting results are shown in Fig. 3(b). The area fraction of the peak at ~397 eV in the corresponding N 1s spectra of Fig. 2(i) and (ii); s_{N3}, assigned to N–Ti–N bonding in nitrogen-substituted TiO_2,[14,15,24] decreased after the 623 K-annealing as displayed

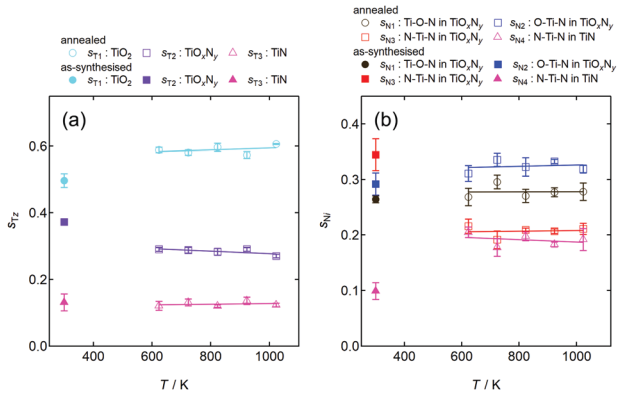

Fig. 3 (open symbols) Area fractions of three and four components in Ti 2p and N 1s region, respectively *versus* annealing temperature [(a) s_{Tz}–T and (b) s_{Ni}–T curves, respectively] calculated from Fig. 2. For reference, the s_{Tz} and s_{Ni} of the as-synthesised TiO_xN_y catalyst are shown by filled symbols.

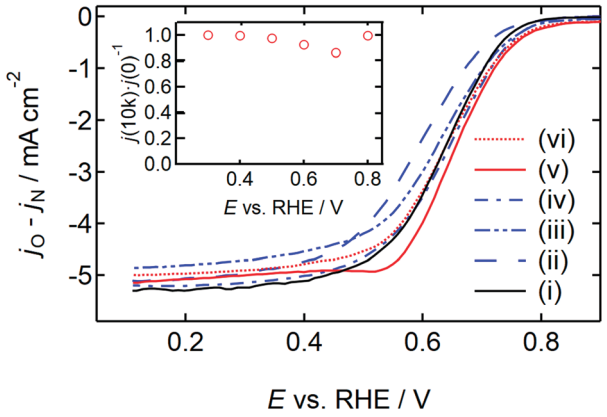

Fig. 4 Rotating disk electrode (RDE) voltammograms of (i) as-synthesised TiO_xN_y catalysts and of those after annealing at (ii) 623 K, (iii) 723 K, (iv) 823 K, (v) 923 K and (vi) 1023 K under 10% H_2 (v/v) in Ar. The scans are performed under N_2 and O_2 atmospheres, with a rotation speed of 1500 rpm and a scan rate of −5 mV s^{-1} (cathodic) in 0.1 mol dm^{-3} H_2SO_4. The inset shows the current density ratio, after to before 10 000 potential cycles *versus* potential [$j(10k)\cdot j(0)^{-1}$ – E] curve of (v).

in Fig. 3(b). These results revealed that some nitrogen atoms, which substituted oxygen atoms in surface TiO_2, were removed after annealing under flowing reductive gas containing no nitrogen source. Moreover, no significant changes were observed in the Ti 2p and N 1s spectra after the annealing temperature increased further, as shown in Fig. 2(ii)–(vi) and Fig. 3(a), (b). Thus, the surface chemical states were almost the same in the five catalysts annealed under an H_2/Ar gas mixture.

Although the annealing temperature did not significantly change the surface chemical states of TiO_xN_y in the temperature range of 623–1023 K, it affected the ORR activity measured using rotating disk electrode (RDE) voltammograms (Fig. 4). The activity of the as-synthesised catalyst decreased after annealing at 623 K, as indicated by the curves in (i) and (ii) of Fig. 4, suggesting that the loss of substitutional nitrogen atoms, as discussed earlier (Fig. 2 and 3), resulted in the loss of active sites, which is in good agreement with the previous studies.[14,15] However, the activity recovered to a level same as that before annealing when the temperature was increased to 823 K and even higher activity was observed at 923 K as shown in Fig. 4(iii)–(v). A further increase in the temperature to 1023 K slightly decreased the activity. The kinetic data are summarized in S3 (ESI†). The durability of the best catalyst, 923 K-sample, was evaluated using a protocol for automotive PEFCs.[4] The potential was cycled between 0.6 V and 1.0 V and the retention rate of current density after 10 000 cycles is shown in the inset of Fig. 4. No significant degradation was observed, which indicates that the active sites produced by the H_2/Ar-annealing were stable under the experimental conditions.

In previous studies on carbon-support-free TiO_xN_y, the activity significantly depended on the amount of substitutionary doped nitrogen atoms.[14,15] From Fig. 2 and 3, the substitutional nitrogen content, s_{N2} + s_{N3}, did not considerably change at 623–1023 K, whereas the activity significantly depended on temperature as shown in Fig. 4. Raman spectroscopy was used

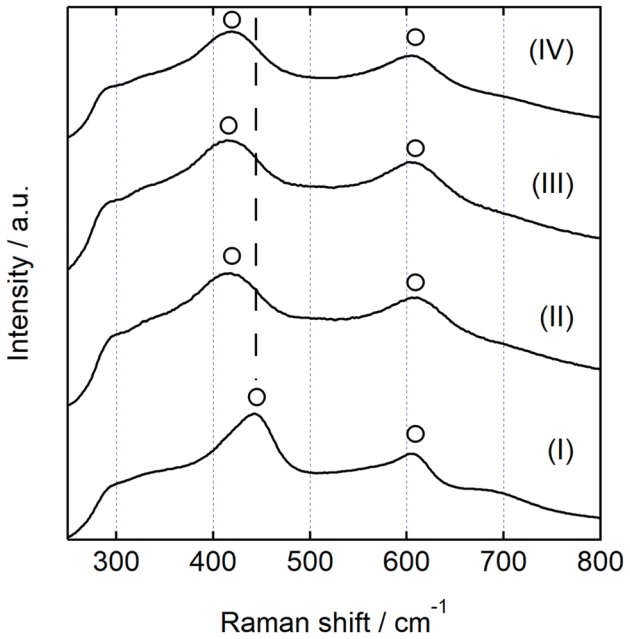

Fig. 5 Raman spectra of (I) commercial rutile TiO_2 powders and TiO_xN_y catalysts after annealing at (II) 723 K, (II) 923 K and (IV) 1023 K under 10% H_2 (v/v) in Ar.

for some catalysts to clarify the source of changes in the activity caused by the annealing temperature. Fig. 5 shows the Raman spectra of three TiO_xN_y catalysts and commercial rutile TiO_2 powders for reference. The commercial TiO_2 powders exhibited two peaks at ~443 and ~606 cm^{-1} in Fig. 5(I), which are typical of the E_g and A_{1g} vibration modes, respectively, of stoichiometric rutile TiO_2.[25,26] The annealed TiO_xN_y catalysts also exhibited two broader rutile peaks, whereas only E_g peaks shifted to lower positions in comparison with commercial rutile TiO_2, as shown in Fig. 5(II)–(IV). The values were ~418, ~414 and ~419 cm^{-1} for the samples at temperatures of 723 K, 923 K and 1023 K, respectively. Both E_g peak shifts, which were not accompanied by the shifts in the A_{1g} peak[25] and peak broadening[26] against the spectrum of the commercial rutile TiO_2, were ascribed to the incorporation of oxygen vacancies. Moreover, the amount of vacancy reached the maximum value at 923 K when the largest peak shift was observed. Based on the results shown in Fig. 1–3, 5 and S1 (ESI†), the bulk of TiO_xN_y particles was TiN and their size did not significantly change due to the low-temperature annealing performed in this study. The surface was oxidised to defective rutile TiO_2 with nitrogen atoms, and the nitrogen doping level deteriorated after H_2 annealing. Although the surface composition was similar in the annealing range of 623–1023 K, the amount of oxygen vacancies depended on the temperature, with the maximum at 923 K. The defective surface is also observed from the transmission electron microscopy (TEM) image shown in Fig. 6.

In most reactions, the reaction rate increases with increasing temperature. The results presented here indicate that the amount of lattice oxygen removed by flowing H_2 in a H_2/Ar gas mixture increased with temperature up to 923 K to form oxygen vacancies.

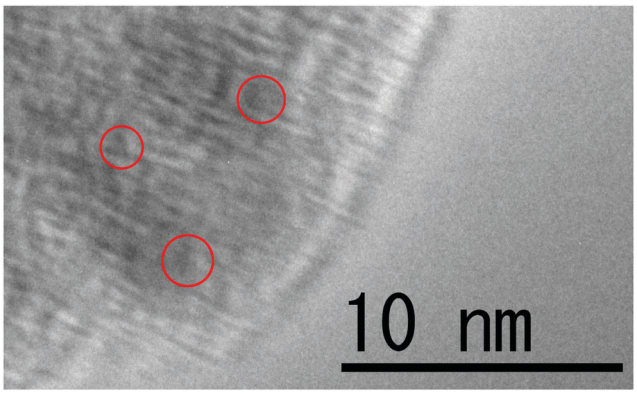

Fig. 6 Transmission electron microscopy (TEM) image of TiO_xN_y catalyst after annealing at 923 K under 10% H_2 (v/v) in Ar. The disordered lattice fringes are indicated by circles.

At a higher temperature of 1023 K, the rate of another reaction, *i.e.* oxidation of TiO_xN_y due to the oxygen contaminants in the mixed gas, was suggested to be higher than the reduction by H_2. As mentioned earlier (Fig. 1), a similar oxidation of hafnium oxynitride by annealing under a flowing H_2/Ar gas mixture has also been reported previously.[22] The charge imbalance caused by the incorporated oxygen vacancies could be compensated by a titanium vacancy and/or oxygen interstitials. The activity exhibited volcano-type dependence on the temperature, which was in good agreement with the amount of oxygen vacancies; the maximum activity was observed at 923 K. The chemical states of the titanium and nitrogen atoms, another factor possibly affecting the ORR activity, did not change with the annealing temperature. Compared with previous studies wherein the presence of oxygen vacancies on TiO_xN_y was discussed using catalysts with various nitrogen doping levels,[14,15] the results of the present study strongly support the hypothesis that oxygen vacancies produced the active sites for the ORR because the nitrogen doping level was kept constant. A low-temperature (923 K) annealing under reductive gas without a nitrogen source, a mixture of H_2 and Ar, was demonstrated to be effective for enhancing both the amount of oxygen vacancies and the resulting activities of the TiO_xN_y catalyst, for the first time. Although the precise role of oxygen vacancy to promote the activity, *i.e.* whether it acted as an O_2 dissociation site by itself or promoted the dissociation and following reaction with protons and electrons indirectly, is not clear at this stage, this new strategy could also be applied to enhance the ORR activity of other oxynitride-type catalysts.

Conclusions

Herein, ORR active sites were created on TiO_xN_y catalysts using reductive annealing performed at temperatures ranging from 623 K to 1023 K without changing the surface composition and chemical states. Both the amount of oxygen vacancies and the activity increased when the temperature was increased up to 923 K without increasing the nitrogen doping level,

which indicates that the oxygen vacancies produced the active sites for the ORR.

Conflicts of interest

There are no conflicts of interest to declare.

Acknowledgements

The author acknowledges Prof Hojun Im and Mr Yusei Tsushima for providing assistance in obtaining the Raman spectra and TEM/FE-SEM images, respectively. This research was partially supported by a Grant-in-Aid for Scientific Research (C), 17K06180, from the Ministry of Education, Culture, Sports, Science and Technology (MEXT) in Japan, a research grant from the Nippon Sheet Glass Foundation for Materials Science and Engineering, a research grant from the Yashima Environment Technology Foundation, Japan and a research grant from Suzuki Foundation, Japan. The XP spectra were acquired at the University of Tokyo, supported by the Nanotechnology Platform of MEXT in Japan.

Notes and references

1 O. Gröger, H. A. Gasteiger and J. P. Suchsland, *J. Electrochem. Soc.*, 2015, **162**, A2605.
2 U. Eberle and R. von Helmolt, *Energy Environ. Sci.*, 2010, **3**, 689.
3 C. E. Thomas, *Int. J. Hydrogen Energy*, 2009, **34**, 6005.
4 A. Ohma, K. Shinohara, A. Iiyama, T. Yoshida and A. Daimaru, *ECS Trans.*, 2011, **41**, 775.
5 B. You, N. Jiang, M. Sheng, W. S. Drisdell, J. Yano and Y. Sun, *ACS Catal.*, 2015, **5**, 7068.
6 G. A. Ferrero, K. Preuss, A. Marinovic, A. B. Jorge, N. Mansor, D. J. L. Brett, A. B. Fuertes, M. Sevilla and Maria-M. Titirici, *ACS Nano*, 2016, **10**, 5922.
7 Y. Chen, S. Ji, Y. Wang, J. Dong, W. Chen, Z. Li, R. Shen, L. Zheng, Z. Zhuang, D. Wang and Y. Li, *Angew. Chem., Int. Ed.*, 2017, **56**, 6937.
8 U. I. Kramm, J. Herranz, N. Larouche, T. M. Arruda, M. Lefèvre, F. Jaouen, P. Bogdanoff, S. Fiechter, I. Abs-Wurmbach, S. Mukerjee and J. P. Dodelet, *Phys. Chem. Chem. Phys.*, 2012, **14**, 11673; M. Kobayashi, H. Niwa, M. Saito, Y. Harada, M. Oshima, H. Ofuchi, K. Terakura, T. Ikeda, Y. Koshigoe, J. Ozaki and S. Miyata, *Electrochim. Acta*, 2012, **74**, 254; D. Singh, K. Mamtani, C. R. Bruening, J. T. Miller and U. S. Ozkan, *ACS Catal.*, 2014, **4**, 3454; Y. Hu, J. O. Jensen, W. Zhang, L. N. Cleemann, W. Xing, N. J. Bjerrum and Q. Li, *Angew. Chem., Int. Ed.*, 2014, **53**, 3675; J. A. Varnell, E. C. M. Tse, C. E. Schulz, T. T. Fister, R. T. Haasch, J. Timoshenko, A. I. Frenkel and A. A. Gewirth, *Nat. Commun.*, 2016, **7**, 12582.
9 A. Zitolo, V. Goellner, V. Armel, M. Sougrati, T. Mineva, L. Stievano, E. Fonda and F. Jaouen, *Nat. Mater.*, 2015, **14**, 937; H. Zhang, S. Hwang, M. Wang, Z. Feng, S. Karakalos, L. Luo, Z. Qiao, X. Xie, C. Wang, D. Su, Y. Shao and G. Wu, *J. Am. Chem. Soc.*, 2017, **139**, 14143; S. H. Ahn, X. Yu and A. Manthiram, *Adv. Mater.*, 2017, **29**, 1606534; H. Shen, E. Gracia-Espino, J. Ma, K. Zang, J. Luo, L. Wang, S. Gao, X. Mamat, G. Hu, T. Wagberg and S. Guo, *Angew. Chem., Int. Ed.*, 2017, **56**, 13800.
10 A. Ishihara, M. Tamura, Y. Ohgi, M. Matsumoto, K. Matsuzawa, S. Mitsushima, H. Imai and K. Ota, *J. Phys. Chem. C*, 2013, **117**, 18837.
11 M. Chisaka, H. Sasaki and H. Muramoto, *Phys. Chem. Chem. Phys.*, 2014, **16**, 20415; D. Sebastián, V. Baglio, S. Sun, A. C. Tavares and A. S. Aricò, *ChemCatChem*, 2015, **7**, 911; F. Wang, H. Li, Q. Wu, J. Fang, Y. Huang, C. Yin, Y. Xu and Z. Luo, *Electrochim. Acta*, 2016, **202**, 1.
12 M. Chisaka, Y. Suzuki, T. Iijima and Y. Sakurai, *J. Phys. Chem. C*, 2011, **115**, 20610; Q. Wu, L. Liao, Q. Zhang, Y. Nie, J. Xiao, S. Wang, S. Dai, Q. Gao, Y. Zhang, X. Sun, B. Liu and Y. Tang, *Electrochim. Acta*, 2015, **158**, 42; M. Chisaka and H. Muramoto, *ChemElectroChem*, 2014, **1**, 863.
13 M. Chisaka, Y. Ando and H. Muramoto, *Electrochim. Acta*, 2015, **183**, 100; M. Chisaka, Y. Ando and N. Itagaki, *J. Mater. Chem. A*, 2016, **4**, 2501.
14 M. Chisaka, Y. Ando, Y. Yamamoto and N. Itagaki, *Electrochim. Acta*, 2016, **214**, 165.
15 M. Chisaka, Y. Yamamoto, N. Itagaki and Y. Hattori, *ACS Appl. Energy Mater.*, 2018, **1**, 211.
16 M. Chisaka, A. Ishihara, H. Morioka, T. Nagai, S. Yin, Y. Ohgi, K. Matsuzawa, S. Mitsushima and K. Ota, *ACS Omega*, 2017, **2**, 678.
17 Y. Du, Z. Dohnálek and I. Lyubinetsky, *J. Phys. Chem. C*, 2008, **112**, 2649.
18 Y. Du, N. A. Deskins, Z. Zhang, Z. Dohnálek, M. Dupuis and I. Lyubinetsky, *Phys. Chem. Chem. Phys.*, 2010, **12**, 6337.
19 S. Wendt, P. T. Sprunger, E. Lira, G. K. H. Madsen, Z. Li, J. Ø. Hansen, J. Matthiesen, A. Blekinge-Rasmussen, E. Lægsgaard, B. Hammer and F. Besenbacher, *Science*, 2008, **320**, 1755.
20 C. D. Valentin, G. Pacchioni, A. Selloni, S. Livraghi and E. Giamello, *J. Phys. Chem. B*, 2005, **109**, 11414; K. Yang, Y. Dai, B. Huang and S. Han, *J. Phys. Chem. B*, 2006, **110**, 24011.
21 M. Chisaka, in *Electrocatalysts for Low Temperature Fuel Cells: Fundamentals and Recent Trends*, ed. T. Maiyalagan and V. S. Saji, Wiley-VCH, Weinheim, 2017, p. 423.
22 M. Chisaka, Y. Suzuki, T. Iijima, Y. Ishihara, R. Inada and Y. Sakurai, *ECS Electrochem. Lett.*, 2012, **1**, F4.
23 K. S. Robinson and P. M. A. Sherwood, *Surf. Interface Anal.*, 1984, **6**, 261; N. C. Saha and H. G. Tompkins, *J. Appl. Phys.*, 1992, **72**, 3072.
24 J. Wang, W. Zhu, Y. Zhang and S. Liu, *J. Phys. Chem. C*, 2007, **111**, 1010; G. Yang, Z. Jiang, H. Shi, T. Xiao and Z. Yan, *J. Mater. Chem.*, 2010, **20**, 5301.
25 J. C. Parker and R. W. Siegel, *Appl. Phys. Lett.*, 1990, **57**, 943; X. H. Wang, J. G. Li, H. Kamiyama, M. Katada, N. Ohashi, Y. Moriyoshi and T. Ishigaki, *J. Am. Chem. Soc.*, 2005, **127**, 10982.
26 R. J. Betsch, H. L. Park and W. B. White, *Mater. Res. Bull.*, 1991, **26**, 613.